Available online at www.sciencedirect.com

SciVerse ScienceDirect

Acta Materialia 60 (2012) 1368–1377

Acta MATERIALIA

www.elsevier.com/locate/actamat

Pristine-to-pristine regime of plastic deformation in submicron-sized single crystal gold particles

Zhang-Jie Wang [a], Zhi-Wei Shan [a,*], Ju Li [a,b,*], Jun Sun [a], Evan Ma [a,c]

[a] Center for Advancing Materials Performance from the Nanoscale (CAMP-Nano) & Hysitron Applied Research Center in China (HARCC), State Key Laboratory for Mechanical Behavior of Materials, Xi'an Jiaotong University, Xi'an 710049, China

[b] Department of Nuclear Science and Engineering and Department of Materials Science and Engineering, Massachusetts Institute of Technology, Cambridge, Massachusetts 02139, USA

[c] Department of Materials Science and Engineering, Johns Hopkins University, Baltimore, Maryland 21218, USA

Received 2 September 2011; accepted 20 October 2011

Abstract

Pristine single crystalline gold particles with sizes ranging from 300 to 700 nm have been fabricated through high-temperature (1150 °C) liquid de-wetting of gold thin films atop a specially designed SiO_2/Si substrate for in situ transmission electron microscopy testing. Quantitative compression tests showed that these particles display cataclysmic structural collapse immediately following elastic loading to very high stresses (over 1 GPa), resulting in a nearly pristine postmortem microstructure despite the large plastic deformation experienced by the particle. This distinct class of dislocation plasticity behavior is attributed to the very high degree of structural perfection of the initial sample, resulting from high-temperature formation or annealing around the melting point. Temporally correlated dislocation nucleation from the contact interface together with the inability to form stable junctions inside is proposed to explain the pristine-to-pristine structural collapse. Upon further compression, once the contact diameter d increases to above a critical value (~250 nm), continuous plastic deformation begins to set in under relatively low flow stress with the postmortem microstructure containing a high density of tangled dislocations, suggesting that a critical dislocation tangling volume under multiple slip is needed for the onset of dislocation storage (robust dislocation jamming) and more conventional plasticity.

Keywords: In situ transmission electron microscopy (TEM); Size dependence; Degree of imperfection (DIP); Robust dislocation jamming; Critical dislocation tangling volume

1. Introduction

Since the micropillar compression experiments of Uchic et al. [1] in 2004, there has been a revived interest in the relationship between the apparent yield/flow strength σ and the size D of surface-confined single crystals, often represented by $\sigma = \sigma_0 + kD^{-\alpha}$ for a certain range of D [2–9]. In addition to obvious dependences on the testing temperature [10], crystal structure [11] and material composition [12], it is important to note that how the surface-confined sample was created in the first place and the resulting surface as well as bulk imperfection conditions have a large effect on the size–strength relationship. For example, in body-centered cubic (bcc) Fe whiskers made with the halide reduction method over half a century ago, a strong size effect on the yield strength was found (see Fig. 8 of Ref. [13]). Similarly, for focused ion beam (FIB) machined Au pillars, ion beam sculpting produces a high density of defects [14] that may impact the development of plasticity upon loading. Therefore large α (~1) was found [11]. In

* Corresponding authors. Address: Center for Advancing Materials Performance from the Nanoscale (CAMP-Nano) & Hysitron Applied Research Center in China (HARCC), State Key Laboratory for Mechanical Behavior of Materials, Xi'an Jiaotong University, Xi'an 710049, China. Tel.: +86 29 82668824; fax: +86 29 82663453 (Z.-W. Shan), tel.: +1 617 253 0166; fax: +1 617 258 8863 (J. Li).

E-mail addresses: zwshan@mail.xjtu.edu.cn (Z.-W. Shan), liju@mit.edu (J. Li).

1359-6454/$36.00 © 2011 Acta Materialia Inc. Published by Elsevier Ltd. All rights reserved.
doi:10.1016/j.actamat.2011.10.035

contrast, the bcc Mo-alloy pillars produced with eutectic solidification by Bei et al. [15,16] show D-independence ($\alpha \approx 0$) over a significant range of D, and simultaneously a very high strength close to the theoretical strength.

One may surmise that in the halide reduction synthesis process, a significant degree of imperfections may still exist inside or near the surface of the whiskers. As Brenner noted, "There appears to be some effect of growth conditions on efficiency in producing strong whiskers. Whiskers grown by precipitation from solution or the reduction of halides show a much larger scatter in strength than the whiskers grown under 'cleaner' conditions, such as deposition in vacuum or inert atmosphere" [13]. In contrast, forming micropillars by eutectic decomposition of liquid alloy is a high-temperature process that could thermally anneal out many imperfections, so much so that even after room temperature (RT) chemical etching, a sample with a lower degree of imperfection (DIP) than Brenner's halide reduction whiskers, and certainly the FIBed pillars, can still be produced. However, the degree of imperfection (DIP) of a sample is more difficult to characterize and quantify than the temperature T or the nominal material composition $\mathbf{X}$: so far it is often expressed vaguely as "pristine" or "non-pristine", which may generate ambiguities. To distinguish different sample conditions, one is therefore tempted to assign a hypothetical DIP scale: DIP = 1 for the materials that are close to ideal crystal, e.g. the samples used by Bei et al. [15,16]. DIP = 2 for materials contain tiny defects, such as point defects, point-defect clusters and even tiny dislocation loops, say a 1 nm radius prismatic loop near the surface produced by point-defect aggregation due to FIB damage. Such tiny dislocation loops near the surface may be irresolvable in transmission electron microscopy (TEM) (not "obvious"), yet from atomistic simulations we know that they could greatly impact the initial plasticity of a sample. Typical examples include the halide reduction whiskers or the FIBed pillars that have experienced thorough mechanical annealing. As Brenner noted [13], "Although whiskers have exhibited the potential strength of perfect crystals, it has not been established whether they are structurally perfect. Structural perfection implies here only the absence of extended defects – in particular, dislocations – and does not include point defects such as vacancies, interstitial atoms, impurities, and electronic defects". DIP > 2 samples are characterized with "obvious" dislocations ("obvious" defined here by the contour length of a dislocation being a significant fraction of D). In general, both DIP = 1 and 2 samples are called as "pristine" crystal. Thus, our definition of "pristine" is identical to Brenner's definition of "structurally perfect". But the new DIP scale is more fine-grained than merely pristine (DIP $\leqslant$ 2) or non-pristine (DIP > 2). This possible distinction in initial sample condition motivated our work at the beginning.

We open our paper by proposing a hypothesis: if a submicron metallic single crystal can achieve DIP = 1, i.e. nearly imperfection-free inside and on the surface (in reference to idealized surfaces), it will exhibit ultra-high strength and a very weak size dependence ($\alpha \approx 0$) [15,16], and also lead to a class of incipient dislocation plasticity behavior (e.g. cataclysmic collapse and critical dislocation tangling volume, to be shown next) that are distinctly different from that of DIP = 2 or DIP > 2 samples. The statement above, regarding low-temperature incipient plasticity due to dislocation slip, is independent of crystal structure. We will attempt to give a theoretical account for this hypothesis at the end of the paper.

Because the hypothesis above is meant to be general, to test it experimentally we choose a material system, sample shape and processing method that are distinct from Mo-alloy pillars [15,16]. We choose a face-centered cubic (fcc) metal, Au, and process it into nano-droplets by liquid de-wetting at a temperature above the melting point of Au and observe its subsequent RT deformation with in situ TEM. We believe our setup is well suited for fundamental studies, because firstly, all metals except Au have an oxidation layer on their surfaces. Therefore, it has been argued that the observed size effect on strength may result from the effect of the surface oxidation layer [17], which would be more difficult to characterize. Second, by studying an elemental metal, no solute effects on dislocation plasticity need to be considered. Lastly, by processing fcc Au with liquid de-wetting, we could achieve well-annealed samples (DIP = 1) to compare with the DIP $\geqslant$ 2 FIBed Au, which showed large α [6], as FIB milling defects are known to affect the mechanical behavior of small sized bcc Mo-alloy pillars [18].

Our in situ TEM tests also facilitate the study of another striking phenomenon in small volume materials: the plastic instability. The plastic instability in small volume material has been widely observed in many materials during compression of micro- and nano-pillars [1,7,15,16,19], compression of nano-particles [20,21], nano-indentation of the thin films [22,23] and well-annealed single crystals [24]. For samples with a certain density of pre-existing mobile dislocations (DIP > 2), the strain bursts were proposed to be caused by the rearrangement of dislocation structure [25] or the destruction of jammed dislocation configurations [26]. For materials with no pre-existing dislocations (DIP $\leqslant$ 2), the onset of plasticity instability is believed to result from dislocation nucleation [23,24]. The common characteristic of these two cases is the collective dislocation behavior, since the creation and motion of a single dislocation (so-called "first dislocation"), even if it moves from one end of the sample to the other end, cannot explain the burst magnitude observed; hundreds of dislocations must be involved to explain the magnitude of the displacement burst. Thus, a mechanism for spatial and temporal correlation, either correlated nucleation or correlated motion of dislocations, must be involved in the discussion of bursts. However, the exact mechanism of strain bursts is still an issue for debate. For example, some authors suggested that the onset of instability was caused by the destruction of a surface oxidation layer [27].

Here in our work, we fabricated DIP = 1 Au particles which can be tested directly in a TEM after fabrication. The particles displayed cataclysmic strain bursts upon the onset of plastic deformation. Our real-time observation of the geometry evolution shows that cataclysmic structural collapse can occur without obvious localized shear offset, rather than associated with the destruction of the surface oxide layer [27]. Combined with postmortem TEM examination of the Au particles at different deformation stages, we proposed that explosive and correlated nucleation of dislocations and their fast escape resulted in the pristine-to-pristine structural collapses observed. Only with subsequent compression to increase the contact diameter to beyond a critical value $d_c \sim 250$ nm, can the nucleated dislocations interact with each other and tangle in the interior of the particle. The continuous, bulk-like plasticity can then set in due to the dislocation storage.

The subsequent content of the paper is organized as follows. In Section 2, we introduce the experimental setup. In Section 3, we describe the experimental findings, and discuss their significance (size independence in burst stress, correlation model for detectable burst, critical contact diameter and dislocation tangling volume for the onset of dislocation storage). In Section 4, we come back to the initial hypothesis and provide theoretical arguments why for DIP = 1 samples the size dependence is very weak.

2. Experimental

The Au nano-particles were fabricated by high-temperature (1150 °C) de-wetting of Au thin films deposited on top of a specially designed silicon wedge substrate (Fig. 1a). A thin SiO_2 layer (Fig. 1b) was deposited first to prevent the reaction between Au and Si by the radio frequency (RF)-magnetron sputtering method. The base pressure and the Ar sputtering pressure were $\sim 6.5 \times 10^{-8}$ mbar and $\sim 5.4 \times 10^{-3}$ mbar, respectively. Au thin film with its thickness ~30 nm was sputter-deposited on thin SiO_2/Si substrate from high-purity Au target (99.99%) under $\sim 4.7 \times 10^{-3}$ mbar Ar pressure (Fig. 1c). The thin Au film was then transferred to another furnace and annealed at 1150 °C in air for 1 h followed by furnace cooling down to room temperature. Because amorphous SiO_2 was liquid-like at the annealing temperature, the Au particles are partially buried inside SiO_2 (Fig. 1d). This helps to fix the particles for the subsequent mechanical tests. The liquid de-wetting [20] of Au films on SiO_2/Si substrate produces particles with random orientation. TEM cross-sectional view examination found that the majority of as-prepared Au particles are single crystal and free of dislocations. This is different from the Au particles fabricated by solid de-wetting on sapphire substrate [21,28,29], which usually contain some dislocations. The Au particles obtained in this work are on the submicrometer scale (average 500 nm) with many showing roughly spherical geometry and a tendency to be polyhedral, as expected from faceting upon solidification. The schematic experimental setup for in situ compression in a TEM is shown in Fig. 1d.

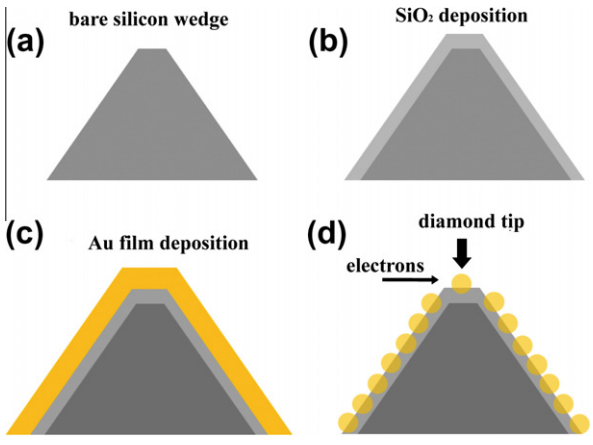

Fig. 1. Schematic showing the experimental design for the in situ compression of gold particle in TEM. (a) Bare silicon wedge. (b) A thin SiO_2 layer is deposited. (c) Thin Au film is deposited on top of the SiO_2/Si wedge. (d) Au particles are formed after high-temperature annealing, and schematic experimental setup for in situ TEM compression test.

The quantitative compression tests inside a TEM (JEM 2100 FEG) were carried out using a Hysitron TEM Pico-Indenter (PI95). The core part of this nano-mechanical testing system is the force/displacement transducer developed by Hysitron [30]. It provides high sensitivity [25] and large dynamic range with maximum force up to 1.5 mN and a linear displacement output up to 5 μm. In the present work, a 1 μm flat punch diamond probe was used. All compression tests were carried out under displacement rate control mode due to its greater sensitivity to transient phenomena [25]. The loading rate was 6 nm s^{-1}. The dynamic deformation process was recorded using a Gatan830 (SC200) CCD camera. It allows one-to-one correlation between the microstructural/geometry evolution and the mechanical data in real time.

3. Results and discussion

Fig. 2a shows the load–displacement curve for a ~500 nm diameter particle. The contact pressure (instantaneous force divided by the instantaneous contact area $\pi d^2/4$, by assuming a circular contact area, where d is the contact diameter directly measured from the recorded images) vs. the compression displacement is shown in Fig. 2b. As shown in Fig. 2a, the loading was elastic up to A, at which point a significant displacement burst occurred at ~2.74 GPa (Fig. 2b), which is close to the theoretical strength of Au (the estimated maximum shear stress $\tau_C \approx G/2\pi = 4.8$ GPa [24,31,32]). The burst displacement along the compression direction was as large as ~45 nm. From the movie (see Supporting material), the Au particle collapses suddenly from Fig. 2d and e. Because the sample collapse rate was far larger than the programmed deformation rate and the limited feedback rate of the testing system, the diamond punch shot out first and then pulled back to regain displacement control under the feedback

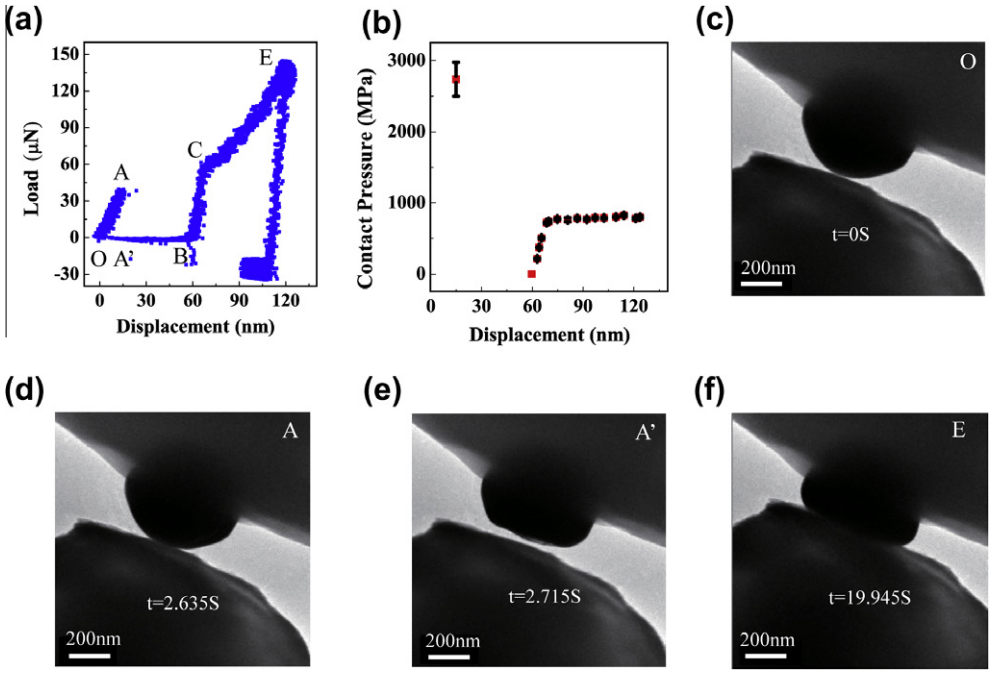

Fig. 2. In situ TEM compression of Au particle (diameter $D = 500$ nm) using a flat diamond punch. (a) Load as a function of displacement. (b) Contact pressure vs. displacement. The error bars in contact pressure is from the uncertainty in measuring particle diameters on the captured images from the movie. Bright-field images of (c) the particle before compression corresponding to O, (d) before burst corresponding to A, (e) after burst corresponding to A′, and (f) at the maximum displacement corresponding to E.

loop. At the same time, the force dropped to zero. The probe then moved forward again to make contact with the particle (point B in Fig. 2a), initiating the second elastic loading, i.e. B to C, after which the particle deformed plastically in a stable and continuous manner, exhibiting typical load–displacement behavior. Fig. 2c–f shows the still frames extracted from the recorded video that correspond to points O, A, A′ and E in Fig. 2a, respectively. The stochastic yielding and strain bursts, followed by stable flow, are very reproducible for particles tested in this work. Typical examples are shown in Fig. 3. Large strain bursts are always observed in the early deformation stage and occur under a high contact pressure (burst pressure), from ~1.1 GPa to ~3 GPa. Such yield strength is consistent with previous nano-indentation results for Au, ranging from 1.7 GPa [33] to 2.5 GPa [34]. For a given particle, the contact pressure at burst decreased along with the deformation if multiple bursts occurred prior to the stable plastic flow (Fig. 3b and h). It was quite interesting to see that contact pressure at the stable plastic flow stage (flow pressure) is almost unchanged for most of the tested particles (Figs. 2b, 3b, e, and h). Presumably this is because the dislocation nucleation/multiplication rate and annihilation rate reach a balance for the given strain rate.

For comparison, the burst and flow pressure vs. particle size are plotted in Fig. 4. No correlation is found between the first burst pressure and the particle size (Fig. 4a), consistent with our opening hypothesis stated in Section 1. As will be explained in detail later, we believe that the cataclysmic first burst arises from temporally correlated dislocation nucleation at the contact interface between the flat punch and Au particle, where the first dislocation nucleation is expected to be the bottleneck. As a result, the burst pressure is more dependent on the crystal orientation and/or surface roughness, rather than the particle size [35]. However, the stable plastic flow pressure (DIP > 2) increases with decreasing particle size (Fig. 4b), as is consistent with the tenet of "smaller is stronger". In order to uncover the microstructure evolution of the particles under compression tests, cross-sectional TEM observations were carried out for different particles at different deformation stages. As shown in Fig. 5a, three typical stages have been identified, i.e. as-prepared stage (S1), after strain burst but before the stable plastic flow stage (S2) and during the stable flow stage (S3). As expected, particles at stage S1 are almost dislocation-free Au crystal (Fig. 5b). This is consistent with the observation that high stresses are necessary to initiate the plastic deformation in such pristine samples. In order to study the corresponding microstructure at stage S2, loading was stopped manually once a burst occurred during the compression test. Surprisingly, postmortem observation found very few dislocations at stage S2, despite the large plastic deformation and the presence of the Au/SiO_2 interface (Fig. 5c). In other words, in terms of microstructural defects, the collapses observed, despite the tremendous plastic strain incurred, left little debris in the interior of the particles, such that the internal structure remains pristine. Of course, while the "before and after" microstructure appears to suggest a pristine-to-pristine evolution, there must have been numerous dislocations

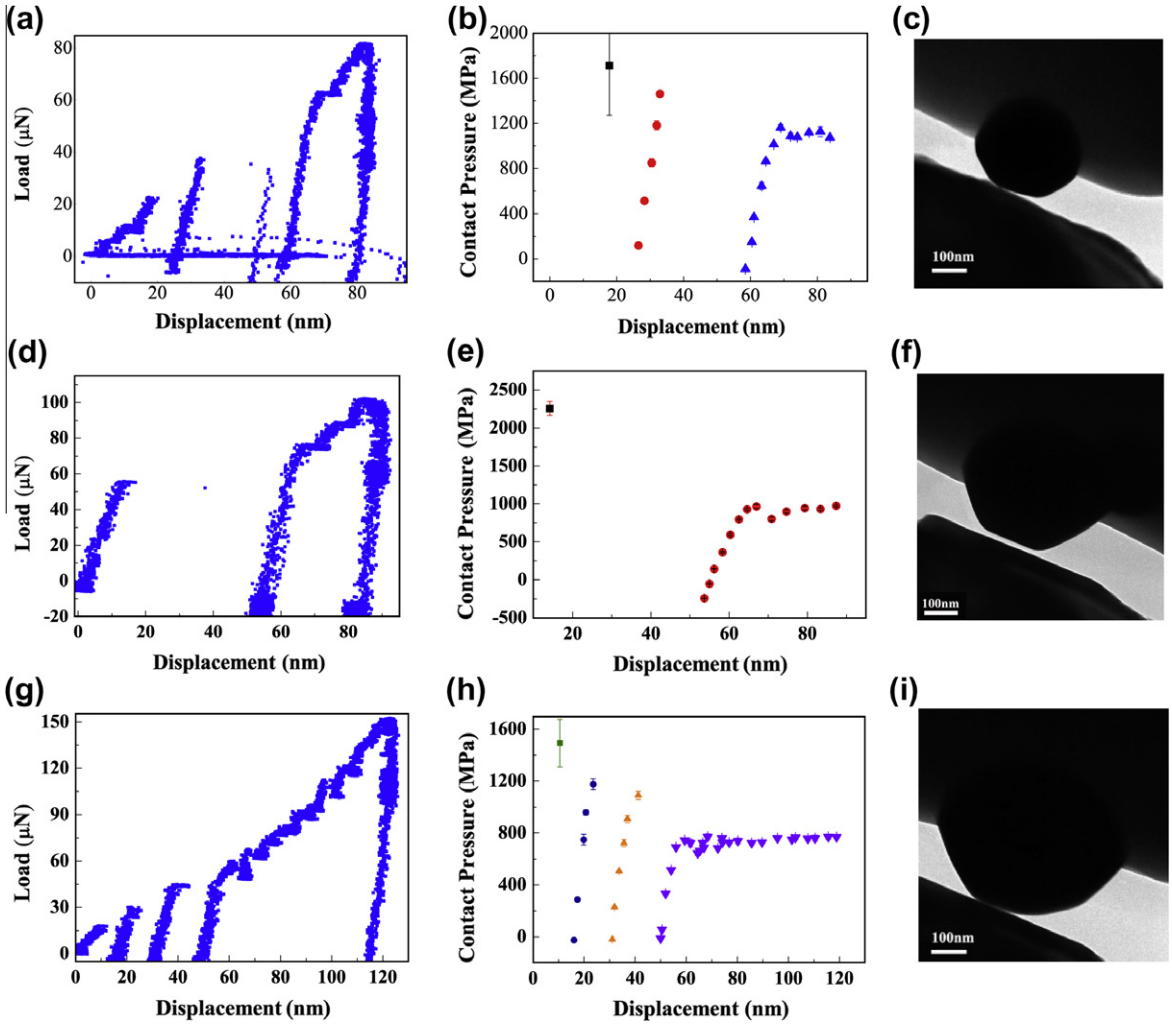

Fig. 3. Typical compression results for Au particles with different sizes. (a) Load vs. displacement. (b) Contact pressure vs. displacement. (c) TEM image of Au particle with $D \approx 300$ nm. (d) Load vs. displacement. (e) Contact pressure vs. displacement. (f) TEM image of Au particle with $D \approx 400$ nm. (g) Load vs. displacement. (h) Contact pressure vs. displacement. (i) TEM image of Au particle with $D \approx 500$ nm.

involved to impart the large shape change associated with the collapse. This indicates that almost all the nucleated dislocations have a very short life time inside the sample volume and must have swept through the particle during the burst before they can tangle with each other to form junctions strong enough to survive in the deforming volume. This is somewhat similar to the scenario in the MD simulation of Mordehai et al. [29], who show that during nano-indentation the dislocations are nucleated and annihilated on the surface, leaving the particle in a dislocation-free state. In contrast, the microstructure of the particle at stage S3 is categorically different. There, high densities of stored/tangled dislocations are observed inside the particle, as shown in Fig. 5d. It is worth noting that the Au/SiO_2 interface appears to be dislocation-transparent because there are almost no blocked dislocations observed near the interface (Fig. 5c and d).

To recap, corresponding to the cataclysmic strain burst and stable plastic flow, the postmortem microstructures are nearly dislocation-free pristine structure and dislocation jammed structure, respectively. Interestingly, some particles burst one time, while some particles burst two or three times (Fig. 3). Further analysis found that the possibility for subsequent strain burst depends on the contact diameter d between the flat diamond punch and the particle during compression (Fig. 6), rather than the particle diameter D. There appears to be a critical value $d_c \sim 250$ nm. Plastic flow is characterized by major strain bursts, and multiple ones, when the contact diameter d is below d_c. Deforming beyond d_c, in contrast, stable and continuous plastic flow takes over. Therefore, the mechanical behavior of Au particles can be divided into two regimes according to the contact diameter. For regime I (i.e. contact diameter is smaller than 250 nm or so), structural collapse occurred by correlated dislocation emissions and fast escapes, while the internal structure goes from pristine to pristine. These dislocation emissions neither started nor ended with an accumulated/jammed dislocation configuration. Yet it must have involved a large number of dislocations and multiple slip systems, to cause the dramatic shape change

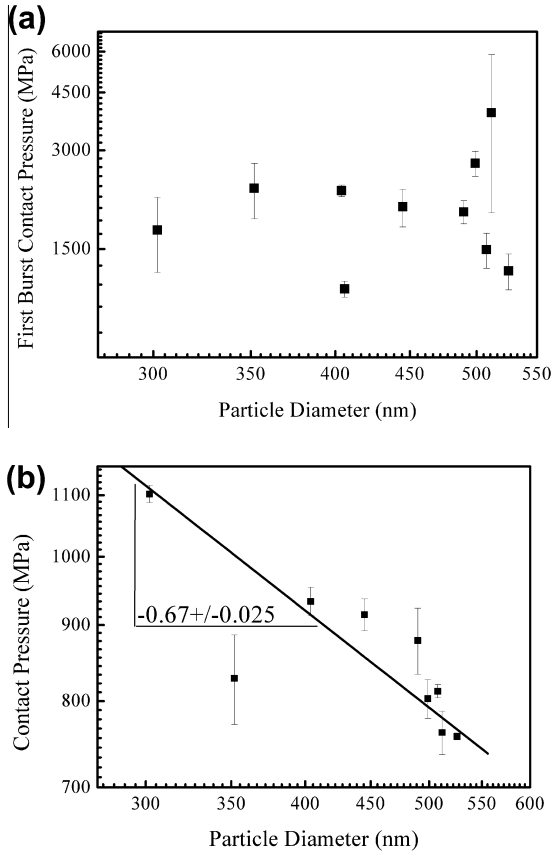

Fig. 4. Size effects on the contact pressure at different deformation stages. (a) The relationship between the contact pressures at collapse vs. the particle diameter. (b) Log–log plot of contact pressure in the continuous deformation stage as a function of particle diameter. The slope for strengthening is ~ -0.67.

in the collapse. For example, for a displacement burst of $\sim$20 nm, at least 100 dislocations would have moved out of the particle. The dislocations appear to have run across the sample without leaving traces. For regime II (i.e. contact diameter is larger than $\sim$250 nm), bulk-like continuous plastic flow will become dominant.

The observed phenomenon can be rationalized by the following mechanism. In regime I, when a pristine crystal is under compression, dislocations preferentially nucleate from the circumference of the contact interface between the sample and the punch, and the nucleation events are correlated temporally as load shedding resulting from emitted dislocations causes neighboring sites to emit dislocations shortly afterwards, and this correlated "infection" process continues rapidly from one site to another, with very short time intervals. The bottleneck of this instability is expected to be the nucleation of the very first dislocation, rather than the correlated events thereafter. As explained in Section 4, this is expected theoretically for DIP = 1 samples with well-annealed surfaces, since the surface sources are uniformly hard to trigger, with a small strain-rate sensitivity $m < 0.1$, which gives a sharp threshold behavior in the first emission rate R vs. σ. In contrast, for DIP = 2 samples, we believe that the easy part is the emission of the first dislocation, as there are many "serendipitous dislocation sources" – imagine, for the sake of argument, random non-"obvious" 1 nm radius prismatic loops near the surface from prior FIB damage, which can easily move under stress – but the hard part (bottleneck) is to have the correlated events thereafter. In short, because plastic instability requires dislocations, but a single dislocation cannot give experimentally detectable bursts, to have a detectable burst requires two things to be true simultaneously, represented by the formula:

$$\text{Probability\_rate\_of\_detectable\_burst} = R(\sigma, D) \times P_{corr}(\sigma, D) \quad (1)$$

where $R(\sigma, D)$ is the probability rate of emitting the first dislocation by pure thermal fluctuation, and $P_{corr}(\sigma, D)$ is the probability of correlated emissions of hundreds of dislocations once the first dislocation has been emitted (the domino effect). Both $R(\sigma, D)$ and $P_{corr}(\sigma, D)$ should monotonically increase with σ. But for "clean" surfaces (DIP = 1), the first term should be the bottleneck; while for "dirty" surfaces, the second term should be the bottleneck.

Consider "clean" surfaces (DIP = 1): in a stress ramp-up experiment, once stress reaches a level where $P_{corr}(\sigma, D) \approx 1$, i.e., were there is a first emission, hundreds of subsequent dislocations would be almost sure to follow. But $R(\sigma, D)$ is exponentially small at this stress level for DIP = 1 samples, so nothing happens. The stress continues to rise in this supersaturated condition until $R(\sigma, D)$ becomes appreciable, at which point the first dislocation can come out with appreciable likeness. The subsequent dislocation emissions shower the sample interior with a high flux of dislocations, leading to a pronounced displacement burst and sample collapse. Correspondingly, the mechanical behavior in regime I is characterized by ultra-high stress to nucleate dislocations from the contact interface and large strain bursts with uncontrollable geometry change.

The pristine-to-pristine mechanism is expected to function only when the crystal is small, i.e. at the micro- or nano-scale. In this case, the small sample volume will have a good chance to be free of easy nucleation sites initially, and the sample can be elastically loaded up to very high stress, at which point new dislocations nucleate from (contact) surfaces and propagate at very high speed [36]. Moreover, the tiny sample size is necessary because the nucleated dislocations must run out of the sample without hitting obstacles or tangling with each other to form robust locks during their life span. If the latter were to happen, for example when two or more dislocations on different slip planes meet to create sessile segments that pin the dislocation forest or function as a sustainable Frank–Read-type source [37], it would lead to internal dislocation multiplication and establishment of dislocation forest, stabilizing the continuous flow. Indeed, this appears to be the mechanism underlying the transition observed between the two stages (S2 and S3 defined in Fig. 5).

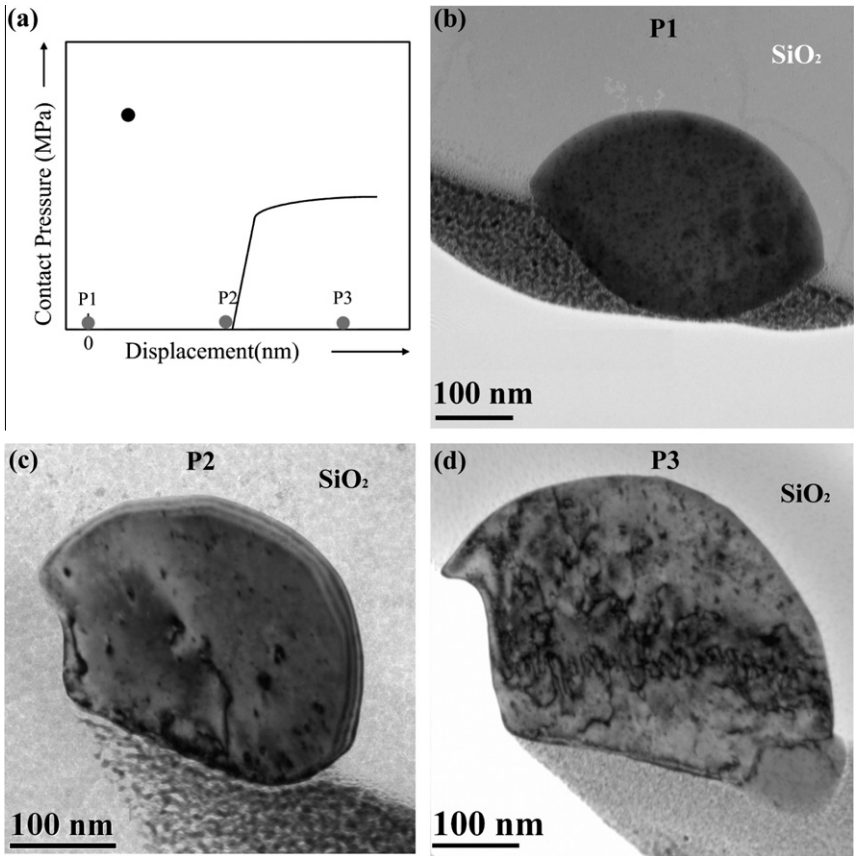

Fig. 5. (a) Schematic showing different deformation stages for postmortem TEM examination. P1, P2 and P3 represent the particle before compression (S1), immediately following strain burst (S2) and after the continuous plastic flow stage (S3), respectively. (b, c and d) are representative bright-field TEM images at stage S1, S2 and S3, respectively.

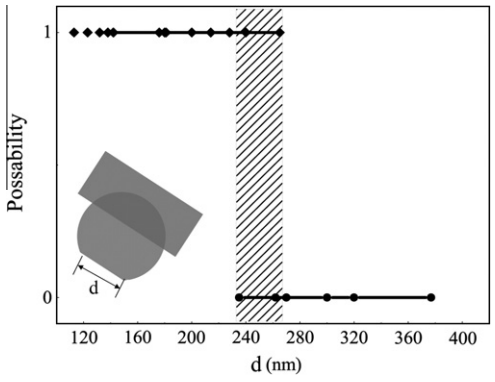

Fig. 6. Probability of the occurrence of the displacement burst/structural collapse during compression of the particles vs. contact diameter. The inset is a schematic defining the diameter of the contact area, d. A critical d_c of ~250 nm separates the two regimes with and without the cataclysmic structural collapses.

In regime II, when the contact diameter exceeds a critical value, the dislocations on two or more slip systems are able to meet and tangle with each other to form stable Frank–Read-type internal dislocation sources that continuously generate dislocations in the interior that counterbalance dislocation loss at the surface and stabilize the dislocation population inside. As a consequence, the programmed displacement rate can be maintained through internal dislocation multiplication and propagation under a relatively low stress level. Note that for the nano-particle under compression, the particle size D has not changed significantly but the contact diameter d between the punch and the particle increases a lot with compression, and the flattening of this contact surface after the major strain bursts results in the transition between the two deformation stages.

We next explain why the transition from pristine-to-pristine bursts to a more continuous plasticity behavior with permanent dislocation storage ("standing army") is dependent on d. As discussed earlier, the dislocations were nucleated at the contact interface triggered by load-shedding elastic interactions. Even though the burst occurred in a very short time, the dislocations nucleated still have a time order. For smaller contact diameter, only limited dislocations will be nucleated at very high stress. Consequently, those dislocations, once nucleated, will move at very high speed and therefore have little chance to meet each other during their life span, especially if they belong to the same slip system since their paths will not intersect. However, with the increase of the contact surface diameter, more nucleation sites will be activated for a given time interval, as shown schematically in Fig. 7. In addition,

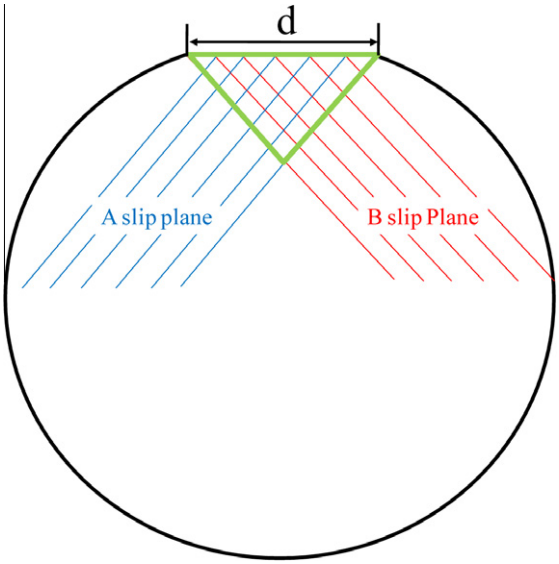

Fig. 7. Cross-sectional schematic of the potential dislocation tangling from intersecting slip systems and dislocation nucleation from contact interface.

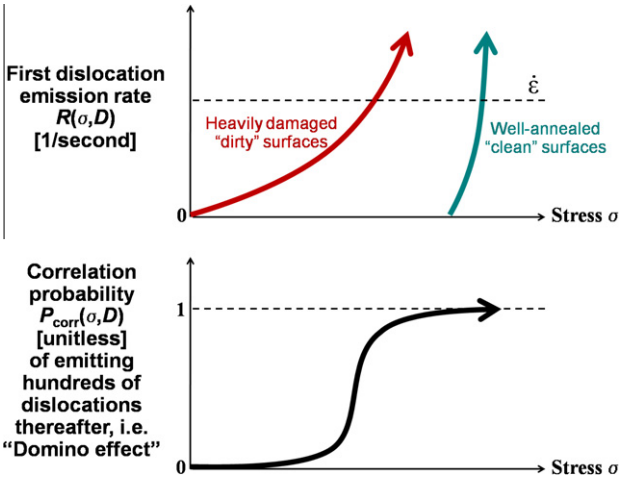

Fig. 8. Illustration of the stress dependence of first dislocation emission rate $R(\sigma, D)$ for well-annealed "clean" (DIP = 1) surface, vs. heavily-damaged "dirty" (DIP = 2) surfaces, in relation to the probability of correlation ("domino effect") $P_{corr}(\sigma, D)$ of emitting hundreds of dislocations after the first dislocation has been emitted.

the crystal volume (marked by triangle in Fig. 7) for potential dislocation tangling between two intersecting slip systems is dependent on the contact diameter as $\propto d^3$. We note that dislocation reactions to form sessile junctions typically happen only between dislocations on two different slip systems. Therefore, with increasing dislocation tangling volume under multiple slip as indicated in Fig. 7, there will be more chances to form dislocation junctions that pin the dislocation forest as well as forming sustainable Frank–Read-type sources. With further compressive displacement and the accompanying increase in d, eventually there will be enough dislocation junctions formed inside the Au sphere to sustain robust dislocation jamming and a stable dislocation population containing both sessile and mobile components (akin to the concept of "standing army"), rendering more stable flow. Apparently the probability for this to happen is 100% once d passes $d_c \sim 250$ nm.

4. Theory behind the opening hypothesis

Several key features distinguish the DIP = 1 incipient plasticity with the more well-known DIP = 2 and DIP > 2 incipient plasticity: ultra-high strength, cataclysmic burst, and weak size dependence of the first burst stress ($\alpha \approx 0$). Below, we would like to explain why our hypothesis is reasonable from theoretical grounds.

The basic nature of an experimentally detectable burst is shown in Eq. (1). A somewhat new concept is $P_{corr}(\sigma, D)$, the probability of correlated emissions of hundreds of dislocations (the domino effect) once the first dislocation is emitted at a given stress (see Fig. 8). In addition to load shedding elastic interactions, correlated emissions could arise due to dislocation kinetic and potential energies in dislocation rebound [38] and deformation twinning [39,40] mechanisms, as well as dislocation self-multiplication mechanism [41] in bcc metals. These correlation mechanisms are often surface/interface mediated, thus introducing D-dependence in $P_{corr}(\sigma, D)$, and also depend on the stress either directly (like load shedding) or indirectly (like via dislocation kinetic energy).

If truly without internal defects at the start of low-T deformation, dislocation plasticity can initiate only after some kind of initial surface dislocation emission. We consider two limiting surface conditions: (a) DIP = 1 samples with nearly ideal microstructure, and (b) DIP = 2 samples where all kinds of tiny imperfections could exist, especially at/near surfaces. According to transition state theory, the probability rate of the very first dislocation emission from a given near-surface site i can be expressed as

$$r_i = \nu_i \exp(-Q_i(\sigma, T, D)/k_B T) \tag{2}$$

where ν_i is the physical trial frequency and $Q_i(\sigma, T, D)$ is the activation free energy [35,42] of heterogeneous dislocation nucleation/emission. The total rate of such first emission is the sum of all microscopic rates:

$$R = \sum_{i \in \text{surface sites}} r_i = \sum_{i \in \text{surface sites}} \nu_i \exp(-Q_i(\sigma, T, D)/k_B T) \tag{3}$$

Within each microscopic rate, the D-dependence should be weak:

$$Q_i(\sigma, T, D) \approx Q_i(\sigma, T) \tag{4}$$

when the activation volume Ω_i [42] of the microscopic process considered (first dislocation emission) is small compared to the sample size, so far-side surface image energetics can be ignored. From atomistic calculations, we know $\Omega = 1 - 10b^3$ (b is full Burgers vector length) near well-annealed surface facets and corners, and Eq. (4) generally holds for D greater than tens of nanometers [35]. Also,

one could best fit the stress-dependent exponential by a power law:

$$\exp(-Q_i(\sigma,T)/k_BT) \approx (\sigma/\sigma_i)^{1/m_i} \tag{5}$$

within a certain range of σ, where σ_i is a characteristic strength of the surface source and

$$m_i \equiv k_BT/\sigma_i\Omega_i \tag{6}$$

is the strain-rate sensitivity of the surface source [35,43].

Furthermore, because of possible rotational and translational symmetries, there can be repeated terms in the Eq. (3) summation, so R sum may be re-grouped as

$$R = \sum_{I\in\text{surface site class}} N_I(D)\nu_I \exp(-Q_I(\sigma,T,D)/k_BT) \tag{7}$$

where I represents a class of surface sites with nearly identical $\{\sigma_i, m_i\}$, and $N_I(D)$ is the multiplicity of sites within each class. Size dependence could indeed arise due to such "entropic" $N_I(D)$ term. Imagine a crystallographically facetted micropillar (aspect ratio fixed) with atomically smooth side facets and corners, then

$$N_I(D) \propto D^{\beta_I} \tag{8}$$

with $\beta = 2$ for heterogeneous dislocation nucleation near class I = surface facet sites, and $\beta = 1$ near class I = surface corner sites.

Formalistically, Eqs. (2)–(7) apply to both (a) and (b) surface conditions. But distinct behaviors could arise from the same equations, resulting in different $R(\sigma)$ dependencies. For DIP = 1 sample surfaces, $\{\sigma_I\}$'s are uniformly very high, approaching the surface ideal strength [44]; and from atomistic calculations of the activation volume [35,43], $\{m_I\}$'s can only be quite low, on the order of 0.01–0.1. Further, the number of surface site classes is small, but the multiplicity within each class is huge. Thus for (a) surfaces, $R(\sigma)$ will manifest a sharp threshold behavior: surface emission is a very rare event if

$$\sigma < \sigma_{th} \equiv \sigma_{I_{dominant}}, \quad I_{dominant} \equiv \underset{I\in\text{surface site class}}{\arg\min} \ \sigma_I \tag{9}$$

with σ_{th} very high. But $R(\sigma)$ will turn sharply on for $\sigma > \sigma_{th}$. In such scenario, scarcity of first dislocation emission is indeed the σ-controlling factor, because unless the sharply defined threshold stress is reached so the first emission can happen, no subsequent events can happen. In such a scenario, in Eq. (1), $P_{corr}(\sigma, D)$ would have already approached ≈ 1 around $\sigma \approx \sigma_{th}$ and its details need not be considered sensitively; by timescale matching argument, the left-hand side of Eq. (1) and therefore R must be fixed to $\sim\dot{\varepsilon}$, where $\dot{\varepsilon}$ is the applied strain rate, for the nucleation rate to be considered "appreciable" [35]. By solving the contour

$$\dot{\varepsilon} = R(\sigma,D) \propto D^{\beta_{I_{dominant}}} \times (\sigma/\sigma_{I_{dominant}})^{1/m_{I_{dominant}}} \tag{10}$$

in $\sigma - D$ space, we could then derive a power-law scaling form:

$$\sigma \propto \dot{\varepsilon}^m D^{-m\beta} \tag{11}$$

where $\{m, \beta\}$ are that of the winning (most easily triggered) surface site class $I_{dominant}$, from which one could derive the formula

$$\alpha = m\beta \tag{12}$$

In view of Eq. (12), the numerical value of α should be low because the m value of a truly microscopic dislocation nucleation process seldom exceeds 0.1 (common value is between 0.01 and 0.05), and β is bounded by 3. So if the strain burst is limited by first dislocation emission, the size sensitivity cannot exceed $\alpha \sim 0.15$. In essence, the activated state of the first dislocation emission is too small to be able to "feel" the size of system.

For (b) surfaces, however, one could argue that a sharp threshold in $R(\sigma)$ cannot exist. This is because the nucleation/emission could be mainly caused by different kinds of structural damage, i.e. "serendipitous dislocation sources", rather than stress. The multiplicity within each site class is small, since each radiation damage is likely different, but the number of distinct classes is huge, with wildly varying σ_i and m_i. The result of summing all these in Eq. (3) is that $R(\sigma)$ is not a sharply thresholded function. In other words, the emission rate of single dislocation is not the bottleneck; $R(\sigma, D) > \sim\dot{\varepsilon}$, even at relatively low stresses. But such single-shot dislocation emissions can hardly register on the experimental load–displacement curve. The experimentally detectable burst arrives only when $P_{corr}(\sigma, D)$ becomes appreciable. Solving the $P_{corr}(\sigma, D) \sim 1$ contour in $\sigma - D$ space gives rise to a different size-dependence characteristics from solving the $R(\sigma, D) \sim \dot{\varepsilon}$ contour for (a). Because the physical mechanisms underlying the dislocation correlation effect [38–40] generally extend to a larger spatial regime than single dislocation emission, one expects a much larger size sensitivity for $P_{corr}(\sigma, D) \sim 1$ contour than for $R(\sigma, D) \sim \dot{\varepsilon}$ contour.

5. Conclusions

In conclusion, we have uncovered two regimes corresponding to different plastic deformation behavior and mechanisms in pristine single crystal Au particles. In regime I, the large strain burst directly following the elastic loading is believed to be due to collective action of dislocations as a result of highly correlated nucleation of dislocations driven by high stresses approaching the theoretical strength. Due to the inadequate chance to meet and form robust dislocation locks, all the dislocations that are generated to mediate the large shape change run out of the sample, leaving behind a pristine microstructure. In contrast, in regime II with larger dislocation tangling volumes between multiple slip systems (larger contact diameter), stable dislocation junction ensemble and Frank–Read-type sources are formed, leading to jammed dislocation configurations readily captured in postmortem examinations. Their occasional and partial destruction only give small bursts at relatively low flow stresses, as reflected by the small stress serrations in the load–displacement curves, instead of cataclysmic

bursts seen in the pristine-to-pristine regime. As such, the mechanism underlying the observed transition between the two regimes at a critical contact diameter is whether or not there is enough tangling volume ($\propto d3$ here, where d is the contact diameter instead of the particle diameter, see Fig. 7) between multiple dislocation slip systems to allow for possible reaction and junction formation to pin the dislocation forest and establish stable and sustainable Frank–Read-type sources inside to replace the surface nucleation controlled plasticity. Based on theoretical arguments and experimental observations, we are able to ascertain that highly perfect metallic single crystals (DIP = 1), produced by high-temperature formation or annealing, indeed give a distinct class of low-temperature incipient plasticity that manifests ultra-high strength, cataclysmic burst, and independence of the first burst stress with D ($\alpha \approx 0$).

Acknowledgements

This work was supported by NSFC (50720145101, 50831004 and 50925104) and 973 Program of China (2010CB631003, 2012CB619402). We also appreciate the support from the 111 Project of China (B06025). Both EM and JL carried out this work under an adjunct professorship at XJTU. JL also acknowledges support by NSF CMMI-0728069, DMR-1008104 and DMR-1120901, and AFOSR FA9550-08-1-0325. EM is supported in part by US-NSF-DMR-0904188.

Appendix A. Supplementary material

Supplementary data associated with this article can be found, in the online version, at doi:10.1016/j.actamat.2011.10.035.

References

[1] Uchic MD, Dimiduk DM, Florando JN, Nix WD. Science 2004;305:986.
[2] Richter G, Hillerich K, Gianola DS, Monig R, Kraft O, Volkert CA. Nano Lett 2009;9:3048.
[3] Kiener D, Grosinger W, Dehm G, Pippan R. Acta Mater 2008;56:580.
[4] Jennings AT, Burek MJ, Greer JR. Phys Rev Lett 2010;104:135503.
[5] Volkert CA, Lilleodden ET. Philos Mag 2006;86:5567.
[6] Greer JR, Nix WD. Phys Rev B 2006;73:245410.
[7] Uchic MD, Shade PA, Dimiduk DM. JOM 2009;61:36.
[8] Gianola DS, Eberl C. JOM 2009;61:24.
[9] Ng KS, Ngan AHW. Acta Mater 2008;56:1712.
[10] Schneider AS, Kaufmann D, Clark BG, Frick CP, Gruber PA, Monig R, et al. Phys Rev Lett 2009;103:105501.
[11] Brinckmann S, Kim J-Y, Greer JR. Phys Rev Lett 2008;100:155502.
[12] Girault B, Schneider AS, Frick CP, Arzt E. Adv Eng Mater 2010;12:385.
[13] Brenner SS. Science 1958;128:569.
[14] Shan ZW, Mishra RK, Asif SAS, Warren OL, Minor AM. Nat Mater 2008;7:115.
[15] Bei H, Shim S, George EP, Miller MK, Herbert EG, Pharr GM. Scripta Mater 2007;57:397.
[16] Bei H, Shim S, Pharr GM, George EP. Acta Mater 2008;56:4762.
[17] Uchic MD, Dimiduk DM, Florando JN, Nix WD. Science 2004;306:1134.
[18] Shim S, Bei H, Miller MK, Pharr GM, George EP. Acta Mater 2009;57:503.
[19] Greer JR, De Hosson JTM. Prog Mater Sci 2011;56:654.
[20] Mook WM, Niederberger C, Bechelany M, Philippe L, Michler J. Nanotechnology 2010;21:055701.
[21] Mordehai D, Lee SW, Backes B, Srolovitz DJ, Nix WD, Rabkin E. Acta Mater 2011. doi:10.1016/j.actamat.2011.04.05.
[22] Lilleodden ET, Nix WD. Acta Mater 2006;54:1583.
[23] Gouldstone A, Koh HJ, Zeng KY, Giannakopoulos AE, Suresh S. Acta Mater 2000;48:2277.
[24] Corcoran SG, Colton RJ, Lilleodden ET, Gerberich WW. Phys Rev B 1997;55:16057.
[25] Minor AM, Asif SAS, Shan ZW, Stach EA, Cyrankowski E, Wyrobek TJ, et al. Nat Mater 2006;5:697.
[26] Csikor FF, Motz C, Weygand D, Zaiser M, Zapperi S. Science 2007;318:251.
[27] Gerberich WW, Kramer DE, Tymiak NI, Volinsky AA, Bahr DF, Kriese MD. Acta Mater 1999;47:4115.
[28] Sadan H, Kaplan WD. J Mater Sci 2006;41:5099.
[29] Mordehai D, Kazakevich M, Srolovitz DJ, Rabkin E. Acta Mater 2011;59:2309.
[30] Warren OL, Shan ZW, Asif SAS, Stach EA, Morris JW, Minor AM. Mater Today 2007;10:59.
[31] Wu B, Heidelberg A, Boland JJ. Nat Mater 2005;4:525.
[32] Asenjo A, Jaafar M, Carrasco E, Rojo JM. Phys Rev B 2006;73:075431.
[33] Kiely JD, Houston JE. Phys Rev B 1998;57:12588.
[34] Wang J, Lian J, Greer JR, Nix WD, Kim K-S. Acta Mater 2006;54:3973.
[35] Zhu T, Li J, Samanta A, Leach A, Gall K. Phys Rev Lett 2008;100:025502.
[36] Gilman JJ. J Appl Phys 1965;36:3195.
[37] Thompson N. Proc Phys Soc B 1953;66:481.
[38] Dregia SA, Hirth JP. J Appl Phys 1991;69:2169.
[39] Zhang JY, Liu G, Wang RH, Li J, Sun J, Ma E. Phys Rev B 2010;81:172104.
[40] Yu Q, Shan ZW, Li J, Huang XX, Xiao L, Sun J, et al. Nature 2010;463:335.
[41] Weinberger CR, Cai W. PNAS 2008;105:14304.
[42] Li J. MRS Bull 2007;32:151.
[43] Zhu T, Li J, Samanta A, Kim HG, Suresh S. PNAS 2007;104:3031.
[44] Dmitriev SV, Kitamura T, Li J, Umeno Y, Yashiro K, Yoshikawa N. Acta Mater 2005;53:1215.